PHYSICAL REVIEW B VOLUME 36, NUMBER 15 15 NOVEMBER 1987-II

Electronic properties of metastable Ge_xSn_{1-x} alloys

David W. Jenkins and John D. Dow
Department of Physics, University of Notre Dame, Notre Dame, Indiana 46556

(Received 21 May 1987)

The energy band gaps and substitutional deep impurity levels of metastable alloys Ge_xSn_{1-x} are predicted. As a function of decreasing alloy composition x the indirect band structure of semiconducting Ge first becomes direct (indicating that Ge_xSn_{1-x} may have applications as an infrared detector) and then metallic. Doping anomalies commonly occur as x decreases. Between $x \simeq 0.4$ and $x \simeq 0.8$, the Gunn effect should occur.

In this paper, we predict the band gaps and substitutional defect levels for alloys of germanium and tin: Ge_xSn_{1-x}. These materials are normally immiscible for most compositions when grown under equilibrium conditions, but have been grown in substitutional, crystalline metastable states for compositions $x > 0.78$ using nonequilibrium growth techniques.[1-3] With increasingly sophisticated growth techniques, we anticipate that metastable Ge_xSn_{1-x} alloys will soon be available for a greater range in x.[4] One purpose of this paper is to outline the electronic structure of these new alloys, and to suggest that, for a restricted range of alloy compositions, they should support Gunn-effect oscillations. Hence we hope to stimulate efforts to grow these materials.

Germanium is an indirect-gap material, the fundamental energy band gap occurring at the L point of the Brillouin zone $[\mathbf{k}=(2\pi/a_L)(\frac{1}{2},\frac{1}{2},\frac{1}{2})]$, with a magnitude of 0.76 eV at low[5] temperature. Tin is a semimetal, a material with no band gap; its valence and conduction bands overlap at the Γ point $[\mathbf{k}=(0,0,0)]$. We predict Ge_xSn_{1-x} to have a fundamental band gap that varies from zero to 0.76 eV as a function of composition x.

I. BAND STRUCTURES

The energy bands of Ge_xSn_{1-x} alloys were predicted using the virtual-crystal approximation and a second-nearest-neighbor tight-binding model of the Koster-Slater type.[6] The parameters, for a first-nearest-neighbor tight-binding Hamiltonian, are taken to be those of Vogl *et al.*,[7] which are known to reproduce valence-band structures and the principal features of the lowest conduction bands for all zinc-blende and diamond covalent semiconductors. An important and nontrivial feature of the Vogl parameters is that they incorporate chemical trends, so changes in these parameters as the semiconductor composition varies are rather well-behaved functions of changes in atomic energies and bond lengths. The Vogl model, in its published form, is lacking two ingredients essential to a proper treatment of Ge_xSn_{1-x} alloys: (i) spin-orbit splitting (which is important for the large-Z Sn atom), and (ii) second-nearest-neighbor parameters (which are needed to correctly simulate the relative conduction-band minimum near point L along Δ). The spin-orbit effect has been incorporated by a number of authors; we share common notation with Ref. 8. Similarly, the second-neighbor interactions can be incorporated as they were for $Si_{1-x}Ge_x$ alloys by Newman and Dow.[9] The resulting Hamiltonian, in a basis of tight-binding states of wave vector $\mathbf{k}$, is

$$H_0(\mathbf{k})=\begin{bmatrix} H_s & 0 & H_{ss}^\dagger & H_{ps}^\dagger \\ 0 & H_p & H_{sp}^\dagger & H_{pp}^\dagger \\ H_{ss} & H_{sp} & H_s & 0 \\ H_{ps} & H_{pp} & 0 & H_p \end{bmatrix},$$

where H_s is

$$\begin{array}{c|cccc|} & |s^*\uparrow\rangle & |s^*\downarrow\rangle & |s\uparrow\rangle & |s\downarrow\rangle \\ |s^*\uparrow\rangle & E_{s^*} & 0 & 0 & 0 \\ |s^*\downarrow\rangle & 0 & E_{s^*} & 0 & 0 \\ |s\uparrow\rangle & 0 & 0 & E_s & 0 \\ |s\downarrow\rangle & 0 & 0 & 0 & E_s \end{array}$$

and H_p is

$$\begin{array}{c|cccccc|} & |\frac{3}{2},\frac{3}{2}\rangle & |\frac{3}{2},\frac{1}{2}\rangle & |\frac{3}{2},-\frac{1}{2}\rangle & |\frac{3}{2},-\frac{3}{2}\rangle & |\frac{1}{2},\frac{1}{2}\rangle & |\frac{1}{2},-\frac{1}{2}\rangle \\ |\frac{3}{2},\frac{3}{2}\rangle & E_p+\lambda & -W_{ps'}g_6/\sqrt{3} & iW_{ps'}g_g/\sqrt{3} & 0 & W_{ps'}g_6/\sqrt{6} & -i\sqrt{2}W_{ps'}g_8/\sqrt{3} \\ |\frac{3}{2},\frac{1}{2}\rangle & -W_{ps'}g_6^*/\sqrt{3} & E_p+\lambda & 0 & iW_{ps'}g_8/\sqrt{3} & 0 & -W_{ps'}g_6/\sqrt{2} \\ |\frac{3}{2},-\frac{1}{2}\rangle & -iW_{ps'}g_8^*/\sqrt{3} & 0 & E_p+\lambda & W_{ps'}g_6/\sqrt{3} & -W_{ps'}g_7/\sqrt{2} & 0 \\ |\frac{3}{2},-\frac{3}{2}\rangle & 0 & -iW_{ps'}g_8^*/\sqrt{3} & W_{ps'}g_6^*/\sqrt{3} & E_p+\lambda & -i\sqrt{2}W_{ps'}g_8/\sqrt{3} & W_{ps'}g_7/\sqrt{6} \\ |\frac{1}{2},\frac{1}{2}\rangle & W_{ps'}g_6^*/\sqrt{6} & 0 & -W_{ps'}g_7^*/\sqrt{2} & i\sqrt{2}W_{ps'}g_8^*/\sqrt{3} & E_p-2\lambda & 0 \\ |\frac{1}{2},-\frac{1}{2}\rangle & i\sqrt{2}W_{ps'}g_8^*/\sqrt{3} & -W_{ps'}g_6^*/\sqrt{2} & 0 & W_{ps'}g_7^*/\sqrt{6} & 0 & E_p-2\lambda \end{array}$$

Here H_{ss} is

$$\begin{array}{c|cccc}
 & |s^*\uparrow) & |s^*\downarrow) & |s\uparrow) & |s\downarrow) \\
\hline
|s^*\uparrow) & 0 & 0 & 0 & 0 \\
|s^*\downarrow) & 0 & 0 & 0 & 0 \\
|s\uparrow) & 0 & 0 & U_{ss}g_0 & 0 \\
|s\downarrow) & 0 & 0 & 0 & U_{ss}g_0
\end{array} ,$$

H_{sp} is

$$\begin{array}{c|cccccc}
 & |\frac{3}{2},\frac{3}{2}) & |\frac{3}{2},\frac{1}{2}) & |\frac{3}{2},-\frac{1}{2}) & |\frac{3}{2},-\frac{3}{2}) & |\frac{1}{2},\frac{1}{2}) & |\frac{1}{2},-\frac{1}{2}) \\
\hline
|s^*\uparrow) & iU_{s^*p}g_4^*/\sqrt{2} & -\sqrt{2}U_{s^*p}g_3^*/\sqrt{3} & iU_{s^*p}g_5^*/\sqrt{6} & 0 & U_{s^*p}g_3^*/\sqrt{3} & -iU_{s^*p}g_5^*/\sqrt{3} \\
|s^*\downarrow) & 0 & iU_{s^*p}g_4^*/\sqrt{6} & -\sqrt{2}U_{s^*p}g_3^*/\sqrt{3} & iU_{s^*p}g_5^*/\sqrt{2} & iU_{s^*p}g_4^*/\sqrt{3} & -U_{s^*p}g_3^*/\sqrt{3} \\
|s\uparrow) & iU_{sp}g_4^*/\sqrt{2} & -\sqrt{2}U_{sp}g_3^*/\sqrt{3} & iU_{sp}g_5^*/\sqrt{6} & 0 & U_{sp}g_3^*/\sqrt{3} & -iU_{sp}g_5^*/\sqrt{3} \\
|s\downarrow) & 0 & iU_{sp}g_4^*/\sqrt{6} & -\sqrt{2}U_{sp}g_3^*/\sqrt{3} & iU_{sp}g_5^*/\sqrt{2} & iU_{sp}g_4^*/\sqrt{3} & -U_{sp}g_3^*/\sqrt{3}
\end{array} ,$$

H_{ps} is

$$\begin{array}{c|cccc}
 & |s^*\uparrow) & |s^*\downarrow) & |s\uparrow) & |s\downarrow) \\
\hline
|\frac{3}{2},\frac{3}{2}) & iU_{s^*p}g_5^*/\sqrt{2} & 0 & iU_{sp}g_5^*/\sqrt{2} & 0 \\
|\frac{3}{2},\frac{1}{2}) & \sqrt{2}U_{s^*p}g_3^*/\sqrt{3} & iU_{s^*p}g_5^*/\sqrt{6} & \sqrt{2}U_{sp}g_3^*/\sqrt{3} & iU_{sp}g_5^*/\sqrt{6} \\
|\frac{3}{2},-\frac{1}{2}) & iU_{s^*p}g_4^*/\sqrt{6} & \sqrt{2}U_{s^*p}g_3^*/\sqrt{3} & iU_{sp}g_4^*/\sqrt{6} & \sqrt{2}U_{sp}g_3^*/\sqrt{3} \\
|\frac{3}{2},-\frac{3}{2}) & 0 & iU_{s^*p}g_4^*/\sqrt{2} & 0 & iU_{sp}g_4^*/\sqrt{2} \\
|\frac{1}{2},\frac{1}{2}) & -U_{s^*p}g_3^*/\sqrt{3} & iU_{s^*p}g_5^*/\sqrt{3} & -U_{sp}g_3^*/\sqrt{3} & iU_{sp}g_5^*/\sqrt{3} \\
|\frac{1}{2},-\frac{1}{2}) & -iU_{s^*p}g_4^*/\sqrt{3} & U_{s^*p}g_3^*/\sqrt{3} & -iU_{sp}g_4^*/\sqrt{3} & U_{sp}g_3^*/\sqrt{3}
\end{array} ,$$

and H_{pp} is

$$\begin{array}{c|cccccc}
 & |\frac{3}{2},\frac{3}{2}) & |\frac{3}{2},\frac{1}{2}) & |\frac{3}{2},-\frac{1}{2}) & |\frac{3}{2},-\frac{3}{2}) & |\frac{1}{2},\frac{1}{2}) & |\frac{1}{2},-\frac{1}{2}) \\
\hline
|\frac{3}{2},\frac{3}{2}) & U_{xx}g_0^* & -U_{xy}g_4^*/\sqrt{3} & iU_{xy}g_3^*/\sqrt{3} & 0 & U_{xy}g_4^*/\sqrt{6} & -i\sqrt{2}U_{xy}g_3^*/\sqrt{3} \\
|\frac{3}{2},\frac{1}{2}) & -U_{xy}g_5^*/\sqrt{3} & U_{xx}g_0^* & 0 & iU_{xy}g_3^*/\sqrt{3} & 0 & -U_{xy}g_4^*/\sqrt{2} \\
|\frac{3}{2},-\frac{1}{2}) & -iU_{xy}g_3^*/\sqrt{3} & 0 & U_{xx}g_0^* & U_{xy}g_4^*/\sqrt{3} & -U_{xy}g_5^*/\sqrt{2} & 0 \\
|\frac{3}{2},-\frac{3}{2}) & 0 & -iU_{xy}g_3^*/\sqrt{3} & U_{xy}g_5^*/\sqrt{3} & U_{xx}g_0^* & -i\sqrt{2}U_{xy}g_3^*/\sqrt{3} & U_{xy}g_5^*/\sqrt{6} \\
|\frac{1}{2},\frac{1}{2}) & U_{xy}g_5^*/\sqrt{6} & 0 & -U_{xy}g_4^*/\sqrt{2} & i\sqrt{2}U_{xy}g_3^*/\sqrt{3} & U_{xx}g_0^* & 0 \\
|\frac{1}{2},-\frac{1}{2}) & i\sqrt{2}U_{xy}g_3^*/\sqrt{3} & -U_{xy}g_5^*/\sqrt{2} & 0 & U_{xy}g_4^*/\sqrt{6} & 0 & U_{xx}g_0^*
\end{array} .$$

We have used the notation of Kobayashi *et al.*[8] for all nearest-neighbor parameters. The second-neighbor parameters are $W_{sp}=4\langle s,\sigma,0\,|\,H_0\,|\,p,\sigma,\mathbf{d}_2\rangle$, where $\mathbf{d}_2$ is the displacement vector of a second neighbor.[10]

The first-neighbor parameters for Ge and Sn were fitted to the band structures of Chelikowsky and Cohen[5] using the method of Kobayashi *et al.*[8] The second-neighbor parameters were fit to the conduction-band edge at the L point using the same band structures. All parameters are given in Table I.

By diagonalizing this Hamiltonian, we obtain the band structures of Ge and Sn, which are in good agreement with the pseudopotential band structures of Chelikowsky and Cohen.[5] (See Figs. 1 and 2.) To obtain the virtual-crystal band structures of $\mathrm{Ge}_x\mathrm{Sn}_{1-x}$ alloys, we first average the parameters of Ge and Sn as follows: on-site parameters, $x[\mathrm{Ge}]+(1-x)[\mathrm{Sn}]$; off-diagonal parameters, $(x[\mathrm{Ge}]\{a(\mathrm{Ge})\}^2+(1-x)[\mathrm{Sn}]\{a(\mathrm{Sn})\}^2)\{a(x)\}^{-2}$; where [Ge] and [Sn] are typical bulk Hamiltonian parameters of Ge and Sn, a(Ge) and a(Sn) are the lattice constants for Ge and Sn, respectively, and we assume Vegard's law:

$$a(x)=xa(\mathrm{Ge})+(1-x)a(\mathrm{Sn}) .$$

This averaging procedure is a virtual-crystal approximation, and is valid because the Onodera-Toyozawa[11] ratio for $\mathrm{Ge}_x\mathrm{Sn}_{1-x}$ is considerably less than 0.1 for the conduction and valence bands. This ratio is the difference δ in on-site energies of the two constituent materials divid-

TABLE I. Sn and Ge tight-binding parameters (in eV, except d, which is in Å). We have added second-neighbor parameters to fit the gap at the L point. The notation is that of Kobayashi *et al.* (Ref. 8).

	Ge	Sn
E_s	-5.8800	-5.8800
E_p	1.5533	1.1733
λ	0.0967	0.2667
E_{s^*}	6.3900	5.9000
U_{ss}	-6.7800	-5.4600
U_{xx}	1.6500	1.4400
U_{xy}	4.8416	3.9042
U_{sp}	4.9520	4.0172
U_{s^*p}	4.5030	3.6459
$W_{ps'}$	0.1352	0.1229
d	2.45	2.81

Additional second-neighbor matrix elements

$$\left(\tfrac{3}{2},\tfrac{1}{2}\,\middle|\,H\,\middle|\,\tfrac{3}{2},\tfrac{3}{2}\right)=-W_{ps'}g_6^*/\sqrt{3}$$

$$\left(\tfrac{3}{2},-\tfrac{1}{2}\,\middle|\,H\,\middle|\,\tfrac{3}{2},\tfrac{3}{2}\right)=-iW_{ps'}g_8^*/\sqrt{2}$$

$$\left(\tfrac{1}{2},\tfrac{1}{2}\,\middle|\,H\,\middle|\,\tfrac{3}{2},\tfrac{3}{2}\right)=W_{ps'}g_6^*/\sqrt{6},$$

$$\left(\tfrac{1}{2},-\tfrac{1}{2}\,\middle|\,H\,\middle|\,\tfrac{3}{2},\tfrac{3}{2}\right)=iW_{ps'}g_8^*\sqrt{2/3}$$

$$\left(\tfrac{3}{2},-\tfrac{3}{2}\,\middle|\,H\,\middle|\,\tfrac{3}{2},\tfrac{1}{2}\right)=-iW_{ps'}g_8^*/\sqrt{3}$$

$$\left(\tfrac{1}{2},-\tfrac{1}{2}\,\middle|\,H\,\middle|\,\tfrac{3}{2},\tfrac{1}{2}\right)=-W_{ps'}g_6^*/\sqrt{2},$$

$$\left(\tfrac{3}{2},-\tfrac{3}{2}\,\middle|\,H\,\middle|\,\tfrac{3}{2},-\tfrac{1}{2}\right)=W_{ps'}g_6^*/\sqrt{3}$$

$$\left(\tfrac{1}{2},\tfrac{1}{2}\,\middle|\,H\,\middle|\,\tfrac{3}{2},-\tfrac{1}{2}\right)=-W_{ps'}g_7^*/\sqrt{2}$$

where

$$g_6=\sin(k_xa/2)\sin(k_ya/2)+i\,\sin(k_xa/2)\sin(k_za/2)$$

$$g_7=\sin(k_xa/2)\sin(k_ya/2)-i\,\sin(k_xa/2)\sin(k_za/2)$$

$$g_8=\sin(k_ya/2)\sin(k_za/2)$$

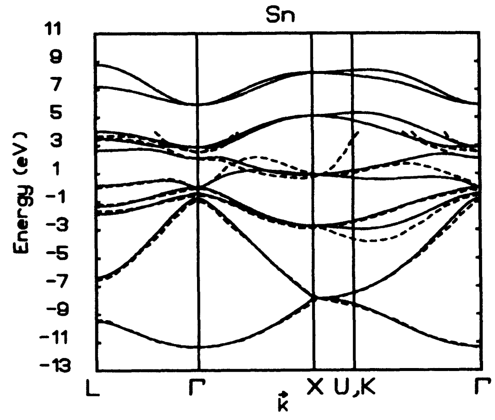

FIG. 2. Band structure of Sn (solid lines) in comparison with the results of Ref. 5 (dashed lines).

ed by the bandwidth W of the associated band. For Ge_xSn_{1-x}, the larger of the differences δ of s and p on-site energies is 0.38 eV. The conduction- and valence-band widths of Sn are 11.34 and 5.72 eV, respectively. (The bandwidths of Ge are comparable.) In this case, for Ge_xSn_{1-x} we have $\delta/W \lesssim 0.02$ for the valence band and $\delta/W \lesssim 0.07$ for the conduction band. These materials satisfy the criterion as well as or better than alloys of GaAs and GaP.

The resulting virtual-crystal-approximation band structures of Ge_xSn_{1-x} are displayed in Figs. 3, 4, and 5 for $x = 0.25$, 0.5, and 0.75, respectively.

Figure 6 displays, as functions of alloy composition x, the principal virtual-crystal band gaps at point Γ, point L, and point X $[\mathbf{k}=(2\pi/a)(1,0,0)]$, and Δ (Δ is the wave vector of the local minimum in the conduction band along the [100] direction; point L is a local minimum).

Interesting features of Fig. 6 are (i) that a direct (Γ)-to-indirect (L) crossover is predicted near $x \simeq 0.8$, (ii) the alloy's fundamental band gap is nonzero for $x > 0.4$, and (iii) the level at Γ is lower in energy than the level at L for $x < 0.8$. This means that Ge_xSn_{1-x} will be semimetallic for $x < 0.4$, a semiconductor with a direct gap for $0.4 < x < 0.8$ (and hence a potential infrared detector or light emitter), and a potential Gunn oscillator for $0.4 < x < 0.8$. (See below.) For $x > 0.8$, Ge_xSn_{1-x} is an indirect-gap semiconductor.

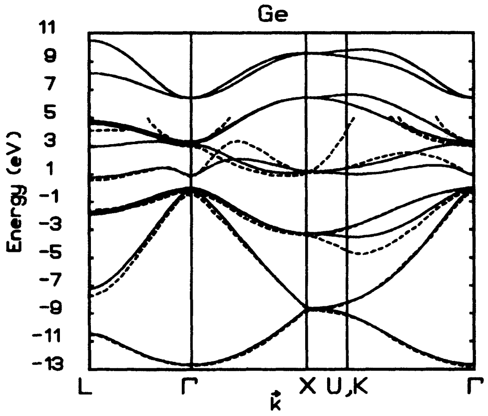

FIG. 1. Band structure of Ge using the present theory (solid lines) compared to the pseudopotential results of Chelikowsky and Cohen (Ref. 5) (dashed lines).

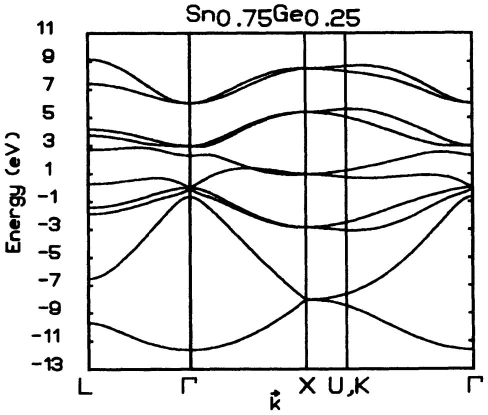

FIG. 3. Band structure of metastable $Ge_{0.25}Sn_{0.75}$.

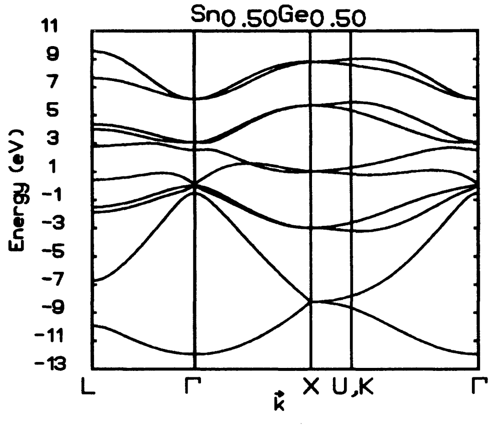

FIG. 4. Band structure of metastable $Ge_{0.5}Sn_{0.5}$.

II. DEEP IMPURITY LEVELS

A. General

The deep impurity levels are computed following the general approach of Hjalmarson *et al.*[7,12] Because of the chemical trends in the matrix elements, a defect potential matrix can be constructed rather easily. For substitutional defects that have the same bond length as the host atoms they replace, the matrix in a basis of localized orbitals centered at the defect site is

$$\begin{array}{c|ccc|} & |E_6) & |E_8) & |E_7) \\ |E_6) & \epsilon_i^s-\epsilon_h^s & 0 & 0 \\ |E_8) & 0 & \epsilon_i^{3/2}-\epsilon_h^{3/2} & 0 \\ |E_7) & 0 & 0 & \epsilon_i^{1/2}-\epsilon_h^{1/2} \end{array} ,$$

where ϵ is the on-site energy[13] of the host (h) or impurity (i). Note that the E_6 state is $s_{1/2}$-like, the E_7 state is $p_{1/2}$-like, and the E_8 state is $p_{3/2}$-like.

The effects of lattice relaxation around the defect and bond-length changes can be incorporated by noting that the off-diagonal matrix elements of the Hamiltonian[13] scale as the inverse square of the bond length. Here we neglect such lattice relaxation effects because (i) they are small, of order 0.1 eV, on the energy scales of relevance to the deep impurity problem—namely, the ~10-eV bandwidths, and the ~1–10-eV scale of the defect potential, and (ii) we are exploring the global chemical trends in the defect levels rather than attempting to predict with precision the energy levels of a specific defect in a single host—while the physics of the unrelaxed deep levels may exhibit well-defined trends, the lattice relaxation may be governed by different chemistry which might obscure the trends in the unrelaxed deep levels.

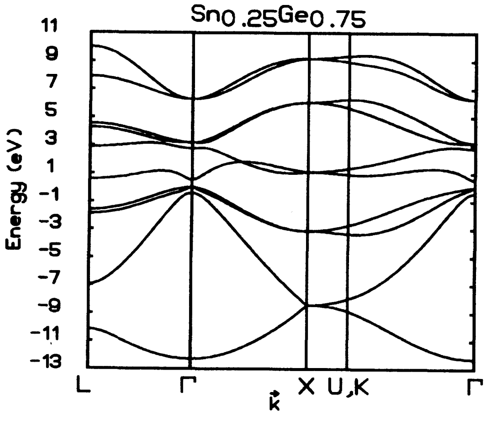

FIG. 5. Band structure of metastable $Ge_{0.75}Sn_{0.25}$.

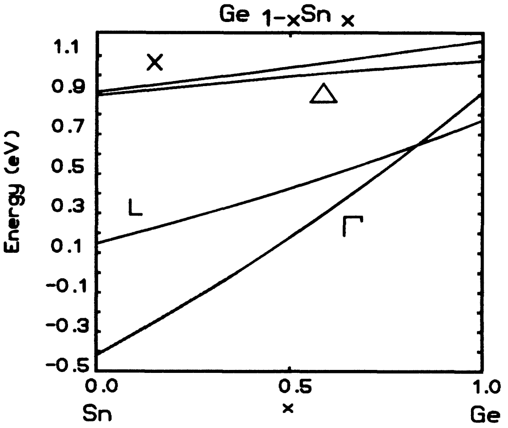

FIG. 6. Predicted lowest conduction bands at Γ, L, and X (the valence band is shaded) vs alloy composition x for Ge_xSn_{1-x}. The band gap varies from zero for $x = 0.4$ to 0.76 eV for pure germanium. This covers energies corresponding to infrared light. The Gunn effect should occur for $0.4 < x < 0.8$ because the high-mobility low-effective-mass Γ minimum lies below the low-mobility L minimum. For $x < 0.4$ the alloy is predicted to have zero gap.

Introducing the Green's-function operator

$$G(E)=(E-H_0)^{-1} ,$$

where the energy E is to be interpreted as having an infinitesimal positive imaginary part when it lies in a host band, the Schrödinger equation for the deep level eigenvalues E is

$$(H_0+V)\psi=E\psi ,$$

and leads to the secular equation

$$\det(1-GV)=0 .$$

Here H_0 is the host-crystal Hamiltonian, $V \equiv H - H_0$ is the defect matrix, and 1 is the unit matrix. Invoking the diamond-crystal symmetry of virtual-crystal Ge_xSn_{1-x}, the secular equations reduce to the scalar equation

$$1/V_s=G_6(E)$$

for the doubly degenerate $s_{1/2}$-like E_6 level,

$$1/V_{1/2}=G_7(E)$$

for the doubly degenerate $p_{1/2}$-like E_7 levels, and

$$1/V_{3/2}=G_8(E)$$

for the fourfold-degenerate $p_{3/2}$-like E_8 levels. Here G_6, G_7, and G_8 are Green's functions for E_6, E_7, and E_8 symmetry, and are defined as follows:

$$G_l(E)=\sum_n \int dk^3 \frac{|\langle l',\mathbf{k},n \mid l',\mathbf{k},n \rangle|^2}{E-E_n(\mathbf{k})} ,$$

where $E_n(\mathbf{k})$ is the nth eigenvalue at wave vector $\mathbf{k}$ and $|l,\mathbf{k},n\rangle$ is the nth eigenvector at $\mathbf{k}$ with $l=s_{1/2}$, $p_{3/2}$, or $p_{1/2}$ for the E_6, E_8, or E_7 symmetry, respectively. The matrix elements V_l are deduced from the chemical trend:[7]

$$V_l=\beta_l(w_{l,\mathrm{imp}}-w_{l,\mathrm{host}}) ,$$

where $w_{l,\mathrm{imp}}$ and $w_{l,\mathrm{host}}$ are atomic energies for the impurity and host atoms, respectively, $l=s_{1/2}$, $p_{3/2}$, or $p_{1/2}$, and $\beta_l=0.8$ for $l=s_{1/2}$, and 0.6 for $l=p_{1/2}$ or $p_{3/2}$. We have $V_{3/2}=V_{1/2}=V_p$.

B. Deep levels

The predicted substitutional-impurity deep-level energies E in the fundamental band gap obtained by solving the secular equations for $\mathrm{Ge}_x\mathrm{Sn}_{1-x}$ are given in Figs. 7 and 8 for levels of E_6, E_7, and E_8 symmetry, respectively. The levels found for Ge are in generally good agreement with what is known about deep impurities in that material. The results of this model are comparable with those of other theories,[14,15] some of which are much more complicated. For example, we calculate the vacancy E_8 level to be 0.24 eV above the valence-band edge, compared to a range from 0.04 to 0.66 eV for other theories.[9] We estimate the uncertainty in our theory to be a few tenths of an eV, comparable with the claimed 0.2-eV uncertainty for self-consistent pseudopotential calculations.[15] In Table II we compare the present theory with experiment. The deep energy levels for S, Se, and Te, all from column VI of the Periodic Table, show a definite trend to higher energies for the series S to Se to Te. This trend is due to a reduction in the magnitude of the atomic orbital energies[7] for the valence electrons of these impurities: hence the defect potential weakens. The trend is present both in theory and in experiment. While the predicted level for S precisely matches experiment (accidentally good agreement for a theory with an uncertainty of a few tenths of an eV), the theory also agrees with the data for Se, and places the Te deep level just above the conduction-band minimum, while the data reveal a level of 0.1 eV below the band edge (within the uncertainty).

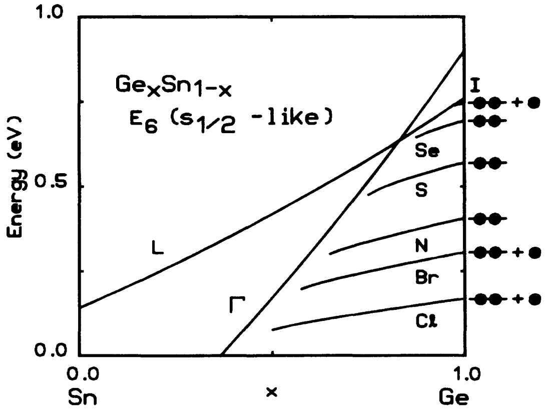

FIG. 7. Predicted substitutional deep impurity levels in $\mathrm{Ge}_x\mathrm{Sn}_{1-x}$ of E_6 (s-like) symmetry as a function of composition x. The zero of energy is the valence-band edge. The conduction-band edges at Γ and L are shown. Impurity levels in the gap for pure Ge are driven into the conduction band as x decreases. Occupancies of the neutral impurity states are shown on the right; electrons are solid circles and holes are open circles. An extra electron (denoted by +●) would occupy a state near the conduction-band edge.

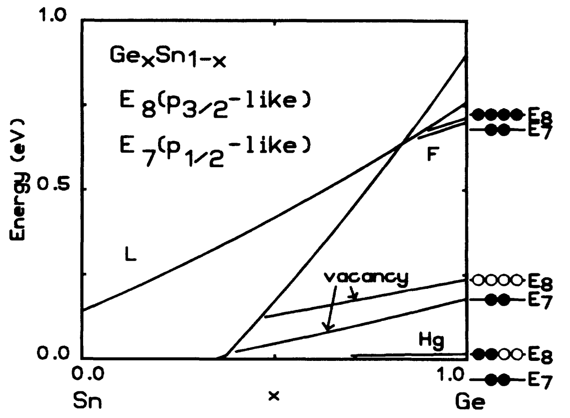

FIG. 8. Predicted substitutional impurity deep levels in $\mathrm{Ge}_x\mathrm{Sn}_{1-x}$ of E_7 ($p_{1/2}$-like) and E_8 ($p_{3/2}$-like) symmetry as functions of composition x. The levels are plotted relative to the valence-band edge. Occupancies of the states are shown; electrons are solid circles and holes are open circles. The conduction-band edges at Γ and L are shown. Impurity levels in the gap for pure germanium are driven into the conduction band as x decreases.

C. Doping anomalies

As the band gap decreases with increasing Sn composition, the deep levels lying in the fundamental band gap of Ge pass into either the conduction band or the valence band of the alloy. When this happens, a doping

TABLE II. Comparison of our calculated deep levels (in eV) in Ge with experimental values taken from W. W. Tyler, J. Phys. Chem. Solids **8**, 59 (1959). The Te deep level in our theory is resonant with the conduction band so the ground state of the Te impurity has its two extra electrons in the effective-mass shallow levels.

Impurity	Deep levels Present theory	Experiment
S	0.58	0.58
Se	0.69	0.62
Te	resonant	0.65

anomaly generally occurs. There are two types of common doping anomalies: (i) deep-shallow transitions, which occur when a deep level crosses a band edge, and (ii) false valences that result from a deep level crossing the fundamental band gap.

For clarity of discussion, we shall assume that the predicted deep-level energies are precisely correct, while cautioning the reader to make allowances for a few tenths of an eV uncertainty in the theory due to neglect of lattice relaxation and charge-state splitting of the levels:[16] for example, the Hg E_8 level, according to Fig. 8, is both an electron and a hole trap, but might actually lie below the valence-band maximum, donating its two holes to the valence band and becoming a double acceptor. (The holes are then trapped by the long-ranged Coulomb potential in shallow acceptor levels.)

1. Deep-shallow transitions

All impurities with deep levels in the gap for Ge undergo a deep-shallow transition as the Sn composition increases. For example, the $p_{3/2}$-like E_8 Hg level is driven into the valence band (Fig. 8), while the other deep levels are driven into the conduction band (Fig. 7.)

When the Cl, Br, and I deep E_6 levels pass into the conduction band with decreasing x, the electrons that occupy the deep levels are autoionized, fall to the conduction-band minimum, and then are trapped in shallow levels. These impurities cease being deep hole traps (plus single donors) and instead become triple donors—the status they would hold in a naive effective-mass theory which contained no deep levels.

Similarly S and Se are deep (double-hole) traps in Ge but become double donors for smaller x (see Fig. 7). N is a deep (electron and hole) trap in Ge, but becomes a shallow donor for $x < 0.6$. The Hg E_8 level traps two electrons and two holes (if the theory is taken literally) in Ge, but Hg becomes a double acceptor with increasing Sn content. Finally the vacancy, which is a deep trap in Ge capable of capturing four electrons or two holes, becomes a double donor when both of its levels enter the conduction band (but is only a hole trap when the E_8 level is in the conduction band and the E_7 level is in the gap).

2. False valences

Substitutional oxygen displays a false valence of zero with respect to Sn or Ge, instead of -2. To see how this happens, consider Fig. 9, which displays the predictions for substitutional impurities from row 2 of the Periodic Table in Ge. The s-like and p-like levels in the conduction band of Ge for a column-IV defect (C) move down in energy as one moves to the right in the Periodic Table. The s-like level lies in the gap for N, but crosses the gap into the valence band for oxygen and F. Similarly the p-like E_7 and E_8 levels descend into the gap for F. Because its s-like E_6 deep level has crossed the gap into the valence band and contains two electrons, neutral oxygen produces neither a double donor (effective-mass intuition) nor a deep trap. Instead neutral oxygen is inert, neither trapping, nor donating, nor accepting electrons. It has a false valence of zero with respect to Ge.

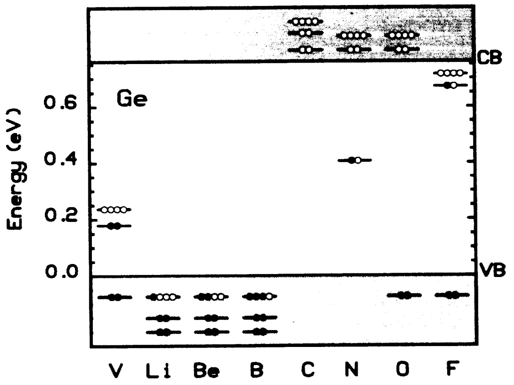

FIG. 9. Predicted deep levels for substitutional impurities from row 2 of the Periodic Table in Ge. Impurities to the right of C, namely N, O, and F, are not donors (counter to intuition). N and F are traps, while O is inert. B and Be are acceptors, C is inert, and Li and the vacancy trap both electrons and holes. Levels in the bands are not to scale.

Similarly F has a false valence of -1 instead of -3, and also has a deep level in the gap of Ge. There are no false valences for impurities on the left side of the Periodic Table, because the filled s- and p-like states in the valence band move up in energy, and cross into the gap for the vacancy levels (Fig. 9).

III. GUNN EFFECT

Gunn oscillations[17,18] result when electrons can transfer from a high-mobility region of the Brillouin zone to a low-mobility region. The mobility is

$$\mu = |e|\tau/m^* ,$$

where e is the electron's charge, and m^* is the electronic

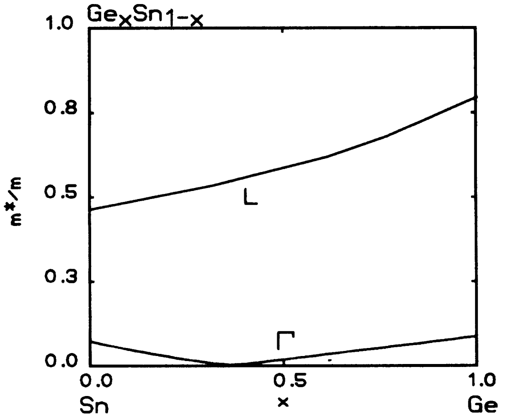

FIG. 10. Predicted effective electron masses in the Γ and L valleys vs composition x. The mass in the Γ valley is smaller than the mass of the L valley, likely resulting in a larger mobility for electrons in the Γ valley. The Gunn effect may be observed for $0.4 < x < 0.8$. The minimum in the mass of the Γ valley occurs at the composition where the energy band gap vanishes.

effective mass, and τ is the scattering time (due to phonon, impurity, and alloy scattering). In most semiconductors the mobility of electrons in the Γ valley of the conduction band is considerably higher than that in the L or X valleys, owing to the very light effective mass. We find this to be the case for Ge_xSn_{1-x} (see Fig. 7).[19] The effective masses produced by the current model may be in error by as much as a factor of 10; nevertheless, the model does give a good qualitative idea of how the masses vary with composition: the mass of the Γ minimum becomes very light near $x \simeq 0.4$, as the alloy becomes metallic (see Fig. 10).

Gunn devices are also known to produce coherent radiation.[20,21] As the potential across the device increases, it eventually causes transitions to the low-mobility state, and then the electrons slow down and form a high-resistivity domain that propagates along the device. Most of the potential drop is over the small domain. The resulting electric fields are large and can cause impact ionization, generating electron-hole pairs. As the domain passes through the material, the electron-hole pairs are left behind. The electrons (holes) fall to the conduction (valence) -band edge through phonon emission. The pairs undergo radiative recombination. Such radiation stimulates further recombination and light is coherently produced. It is an unanswered experimental question whether such effects occur in Ge_xSn_{1-x}.

IV. SUMMARY

In summary, we have predicted the electronic structure of Ge_xSn_{1-x} alloys, and find that these materials should exhibit interesting properties for some ranges of composition x, including direct band gaps in the infrared and band structures compatible with the Gunn effect. We hope that this work will stimulate further attempts to produce electronic-grade Ge_xSn_{1-x} materials.

ACKNOWLEDGMENTS

We are grateful to L. Romano, K. Newman, and D. Vasquez for their many useful discussions, and we gratefully acknowledge the generous support of the U.S. Office of Naval Research (under Contract No. N00014-84-K-0352). One of us (J.D.D.) thanks the Department of Chemical Engineering and Materials Science of the University of Minnesota for their hospitality.

---

[1] *Handbook of Binary Metallic Systems (Structures and Properties) 2* (Israel program for Scientific Translations, Jerusalem, 1967).

[2] S. Oguz, W. Paul, T. F. Deutch, B.-Y. Tsaur, and D. V. Murphy, Appl. Phys. Lett. **42**, 848 (1983).

[3] L. Romano, J. E. Sungren, S. A. Barnett, and J. E. Greene, J. Cryst. Growth (to be published).

[4] Compositions with $x \simeq 0$ have not, to our knowledge, been attempted.

[5] J. R. Chelikowsky and M. L. Cohen, Phys. Rev. B **14**, 556 (1976).

[6] J. C. Slater and G. F. Koster, Phys. Rev. **94**, 1498 (1954).

[7] P. Vogl, H. P. Hjalmarson, and J. D. Dow, J. Phys. Chem. Solids **44**, 353 (1983).

[8] A. Kobayashi, O. F. Sankey, and J. D. Dow, Phys. Rev. B **25**, 6367 (1982). Note that in this paper the definitions for $g_4(\mathbf{k})$ and $g_5(\mathbf{k})$ are different from ours. Our definitions are $g_4(\mathbf{k})=g_2(\mathbf{k})+ig_1(\mathbf{k})$ and $g_5(\mathbf{k})=g_2(\mathbf{k})-ig_1(\mathbf{k})$.

[9] K. E. Newman and J. D. Dow, Phys. Rev. B **30**, 1929 (1984).

[10] Additional second-neighbor parameters are listed in Table I. There are 12 second-neighbor vectors related by symmetry. One vector is $\mathbf{d}_2=a_L(\frac{1}{2},\frac{1}{2},0)$, where a_L is the lattice constant.

[11] Y. Onodera and Y. Toyozawa, J. Phys. Soc. Jpn. **24**, 341 (1968).

[12] H. P. Hjalmarson, P. Vogl, D. J. Wolford, and J. D. Dow, Phys. Rev. Lett. **44**, 810 (1980). See also W. Y. Hsu, J. D. Dow, D. J. Wolford, and B. G. Streetman, Phys. Rev. B **16**, 1597 (1977).

[13] W. A. Harrison, *Electronic Structure and the Properties of Solids* (Freeman, San Francisco, 1980), p. 48ff.

[14] For a recent review of deep-level theories, see S. Pantelides, Rev. Mod. Phys. **50**, 797 (1977).

[15] See Table II of Ref. 9.

[16] S. Lee, J. D. Dow, and O. F. Sankey, Phys. Rev. B **31**, 3910 (1985).

[17] B. E. Streetman, *Solid State Electronic Devices,* (Prentice-Hall, Englewood Cliffs, New Jersey, 1980), p. 47.

[18] J. B. Gunn, Suppl. J. Phys. Soc. Jpn. **21**, 505 (1966).

[19] The calculated effective masses differ from experimental values (0.02 for Sn at point Γ and 0.08 for Ge at point L [see J. I. Pankove, *Optical Processes in Semiconductors* (Dover, New York, 1971), p. 410]), being 0.08 and 0.79 for Ge and Sn, respectively.

[20] J. I. Pankove, *Optical Processes in Semiconductors* (Dover, New York, 1971), p. 247.

[21] See, for example, A. C. Chynoweth, W. L. Feldmann, and D. E. McCumber, Suppl. J. Phys. Soc. Jpn. **21**, 514 (1966).

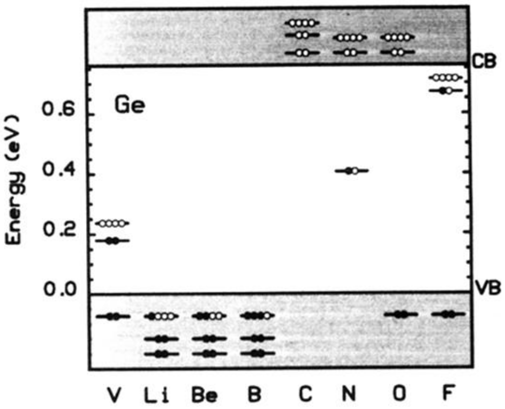

FIG. 9. Predicted deep levels for substitutional impurities from row 2 of the Periodic Table in Ge. Impurities to the right of C, namely N, O, and F, are not donors (counter to intuition). N and F are traps, while O is inert. B and Be are acceptors, C is inert, and Li and the vacancy trap both electrons and holes. Levels in the bands are not to scale.